2021 43rd Annual International Conference of the
IEEE Engineering in Medicine & Biology Society (EMBC)
Oct 31 - Nov 4, 2021. Virtual Conference

An Automated Workflow for the Electric Field Modeling of High-definition Transcranial Direct Current Stimulation (HD-tDCS) in Chronic Stroke with Lesions

Vikram Shenoy Handiru[1,2], Danit Mark[1], Armand Hoxha[1], and Didier Allexandre[1,2]

Abstract— **Transcranial Direct Current Stimulation is a popular noninvasive brain stimulation (NIBS) technique that modulates brain excitability by means of low-amplitude electrical current (usually <4mA) delivered to the electrodes on the scalp. The NIBS research has gained significant momentum in the past decade, prompting tDCS as an adjunctive therapeutic tool for neuromuscular disorders like stroke. However, due to stroke lesions and the differences in individual neuroanatomy, the targeted brain region may not show the same response upon NIBS across stroke patients. To this end, we conducted a study to test the feasibility of targeted NIBS. The hand motor hotspot (HMH) for each chronic stroke participant was identified using Neuronavigated Transcranial Magnetic Stimulation (TMS). After identifying the HMH as the neural target site, we applied High-definition TDCS with the current delivered at 2mA for 20 minutes. To simulate the effects of HD-tDCS in the brain, especially with stroke lesions, we used the computational modeling tool (ROAST). The lesion mask was identified using an automated tool (LINDA). This paper demonstrates that the stroke lesions can be incorporated in the computational modeling of electric field distribution upon HD-tDCS without manual intervention.**

Clinical relevance— **Our proposed automated workflow opens up the possibility of individualized tDCS dosage calibration for neuropathological conditions, including stroke and TBI.**

I. INTRODUCTION

Transcranial Direct Current Stimulation (tDCS) is a promising neuromodulation tool that is gaining significant attention in clinical research spanning psychiatry [1] and neurorehabilitation [2], [3]. However, tDCS for clinical use is still in its infancy as tDCS yielded mixed results regarding the significant improvement in functional outcomes [4], [5]. We attribute this observation to the lack of understanding of the exact mechanism of brain stimulation in the clinical population. Furthermore, given the heterogeneity in stroke in terms of lesion location, we need a targeted approach wherein we stimulate more focal regions in the brain. This will further help us elucidate the underlying mechanism of tDCS in the specific region of interest. Recent advances in the development of High-definition tDCS (HD-tDCS) show that HD-tDCS is spatially focal and can potentially be used for targeted stimulation of the affected region in the brain [6]. Moreover, HD-tDCS is shown to have longer effects in terms of cortical plasticity as compared to the conventional sponge-electrode tDCS [7]. However, the benefits of HD-tDCS for motor recovery in stroke are not fully explored. Given the high focality of HD-tDCS, structural brain anomalies such as lesions or tumors can affect the electric field intensity at the target site. This poses a challenge in understanding whether the targeted region on the ipsilesional side is getting the electric field intensity delivered. The precise pattern of electrical current flow is influenced by many factors, including the stimulation intensity, stimulation site on the scalp, the neuroanatomy of the individual getting the stimulation, and the tissue properties in the brain. The computational models need to consider these factors, mainly when dealing with anatomies with a pathological condition. It is reported that the cerebrospinal fluid is highly conductive [8] in terms of the electric current flow within the brain, and the structural changes such as cerebral edema caused by hydrocephalus can result in abnormally high/low current in the target region. By measuring the deviation of electric field flow characteristics, we can personalize the tDCS dosage. This paper presents an automated workflow for the computational modeling of electric field flow in chronic stroke with lesions. Our workflow allows for estimating the current flow in any given anatomical region of interest with the volumetric approach.

II. METHODS AND MATERIALS

A. Participants

Seven (4 Male, 3 female) chronic stroke survivors (Age: 58.85 ± 6.12 years) participated in this study. The study was approved by the Kessler Foundation Institutional Review Board. All participants who volunteered for the study consented and were screened for eligibility. The main inclusion criteria were chronic stroke (stroke onset at least six months before the consenting date) and have complaints of poor hand dexterity. Patients with severe wrist spasticity scores >3 (Modified Ashworth Scale) were excluded in addition to any contraindications to TMS, tDCS, and MRI [9], [10].

B. MRI Data Acquisition and Processing

The MRI data of each participant was obtained at the Rocco Ortenzio Neuroimaging Center at Kessler Foundation

*This study was supported by New Jersey Health Foundation (Grant PC 9-19)

[1]V. Shenoy Handiru, D. Mark, A. Hoxha, and D. Allexandre are with the Center for Mobility and Rehabilitation Engineering Research, Kessler Foundation, West Orange, New Jersey, USA 07052. [2]V. Shenoy Handiru, and D. Allexandre are also affiliated with the Department of Physical Medicine and Rehabilitation, Rutgers New Jersey Medical School, Newark, NJ, USA.

Corresponding author is V. Shenoy Handiru (Ph: 973-324-3578) and Email: vshenoy@kesslerfoundation.org

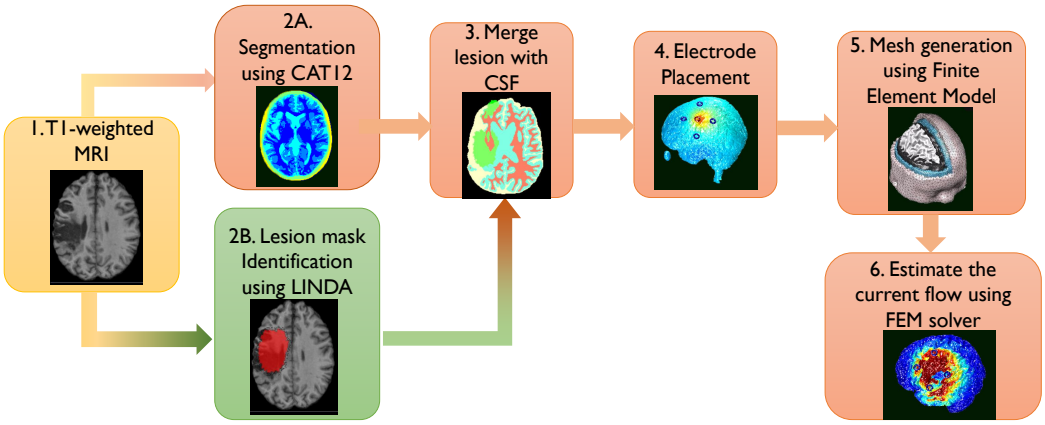

Fig. 1. The proposed workflow for the computational modeling of HD-tDCS in chronic stroke with lesions

using a Siemens Skyra 3T scanner (Erlangen, Germany). The T1-weighted structural MRI scans were collected with the specification as follows: 1-mm isotropic voxel resolution, TE = 3 ms, TR = 2300 ms, 1-mm thick 176 slices, Field of View (FOV) 256x256 mm^2.

C. Identification of the motor hotspot using TMS Neuronavigation

After the participant underwent an MRI scan, his/her motor hotspot corresponding to the First Dorsal Interosseous (FDI) muscle was identified using Transcranial Magnetic Stimulation (TMS). Subject-specific MRI was used for the Neuronavigation system Brainsight (Rogue Research Inc, Montreal, Canada) for TMS navigation. Neuronavigation TMS using a figure of 8 coils (D70^2, Magstim) was applied over the hand knob region of the ipsilesional motor cortex (close to the electrode C3/C4 region contralateral to the paretic arm) to probe for the location that produces maximal Motor Evoked Potential (MEP) from the FDI muscle using the standard relative frequency procedure [11]. Surface electromyography (EMG) was recorded from the paretic FDI using a pair of Ag/AgCl electrodes in a belly-tendon montage during an index finger abduction task using the data acquisition system Powerlab from ADintruments (Sydney, Australia). A site was identified as the target of interest for TMS if an MEP (amplitude $>$ 50 uV peak-to-peak) was found for at least 6 out of 10 trials.

Using a grid-search approach, we probed the neighboring sites and marked the one as Hand Motor Hotspot (HMH) if it produced the MEP at the minimum single-pulse stimulator output intensity. If we could not identify the HMH at rest, we tried to hunt for the motor hotspot during submaximal contraction (20% of the maximum voluntary contraction of the FDI muscle). The site was considered the 'active HMH' if the stimulation produced an EMG output of 0.1mV larger than the background EMG during submaximal contraction. The HMH coordinates obtained from the Brainsight Neuronavigation software were then transformed to MNI coordinates.

D. Computational Modeling of HD-tDCS

In the proposed workflow shown in Fig. 1, we mainly used the ROAST software (https://www.parralab.org/roast/), which follows a realistic volumetric approach to model the electric field distribution. As an end-to-end pipeline, the ROAST toolbox can automatically process individual MRI scans to generate the 3D rendering of the electric field (EF) distribution in the brain. As the electric field distribution is affected by different layers in the brain, the conductivity values are considered during the segmentation process handled by the SPM12 toolbox (https://www.fil.ion.ucl.ac.uk/spm). We used the default conductivity values recommended in ROAST (white matter 0.126 S/m, gray 0.276 S/m, cerebrospinal fluid 1.65 S/m, bone 0.01 S/m, skin 0.465 S/m, air 2.5e-14 S/m, gel 0.3 S/m, and electrode 5.9e7 S/m) [12] to obtain the e-field distribution in different layers. Once the segmentation is done using the CAT12 tool within SPM12 (Step 2A in Fig. 1), the ROAST applies the user-defined parameters (such as the electrode montage, electrode shape, current intensity, etc.) in its getDP solver (Step 6) to solve the governing equations of EF distribution. As a deviation from the regular workflow, which is sufficient for the computational modeling in healthy brains, we now present the integration of lesion segmentation with the ROAST software (Step 3 in Fig. 1).

We used an automated approach to segment the chronic stroke lesions in T1-weighted MRI using the LINDA (Lesion Identification with Neighborhood Data Analysis) toolbox available publicly [13]. The toolbox is made publicly available `http://dorianps.github.io/LINDA/`. The conductivity values of the lesion were tested for different values (white matter, gray matter, and CSF) to assess the effect of lesion on the EF distribution after HD-tDCS. As ischemic stroke often results in cerebral edema, which further causes the cerebrospinal fluid to fill the vacuum [14], we believe the lesion conductivity values may be similar to that of CSF. We highlight that the lesion modeling is done such that the lesion is located over the left hemisphere mainly because the LINDA model is trained using the stroke MRIs with left lesions. For subjects with a

lesion on the right hemisphere, the MR images were flipped along the midline so that the lesion appeared on the left hemisphere for all subjects.

In Step 4 (Fig. 1), the following configuration for Anodal High-definition Transcranial Direct Current Stimulation (Anodal HD-tDCS) was used: 4 × 1 ring electrodes were placed over the ipsilesional area. For the simulation purpose, we place the anodal electrode over the HMH identified using TMS (explained earlier in subsection II.C), and 4 cathodes were placed around the HMH in a 10-10 EEG montage setup. The landmarks (nasion, left, and right preauricular points) were previously identified during the TMS visit. In the absence of Neuronavigated HMH, one can use the 10-10 EEG montage setup with C3 as the anode and FC3, CP3, C1, and C5 as cathodes (if targeting left hemisphere). The current injected was set at 2mA for the anode (C3), and the outgoing current at each of the cathode was -0.5mA. All these ring electrodes have an outer diameter of 12 mm, an inner diameter of 6 mm, and a thickness of 1 mm. In Step 5 (Fig. 1), a finite element mesh is generated using iso2mesh within the roast tool. Since our goal is to assess the effect of HD-tDCS on the motor behavior in chronic stroke, we additionally processed the EF distribution in the targeted ipsilesional primary motor (M1) area by creating a mask of the corresponding Brodmann Area 4 using the WFU Pickatlas ROI selection tool [15]. As the ROIs are defined on the MNI152 template, we coregistered all the results (including the lesion mask and the EF intensity values) to the MNI152 template. Finally, we obtained the EF distribution in the brain tissues (gray and white matter) comprising the M1 area. The results were also validated using another software, SIMNIBS 3.2.4, by following the pipeline [16].

III. Results

The results of the lesion segmentation are shown in Fig. 2 for those stroke subjects who had lesions in the M1 region. The motor impairment in other cases could be due to the subcortical stroke affecting the corticospinal tract. For the sake of simplicity, we present the lesion mask identified using LINDA, which is observable in the vicinity of the M1 region on the cortical surface.

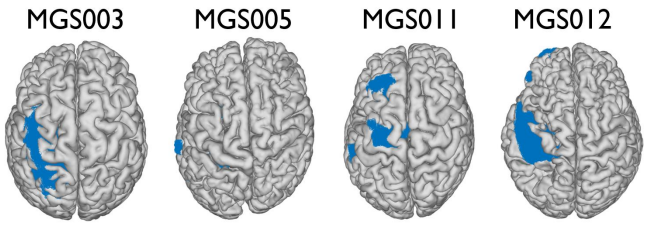

Fig. 2. Cortical surface generated after integrating the lesion mask generated using LINDA toolbox.

The results of the electric field and current density magnitude are shown for one of the subjects (MGS012) in Fig. 3. In Fig. 3A, the histogram distribution of EF intensity values is presented for white and gray matter and highlights the peak EF magnitude. Fig. 3B illustrates the visualization of EF magnitude on the targeted site, and Fig. 3C presents the current flow in different axes.

TABLE I

MNI coordinates of the hand motor hotspot identified using TMS neuronavigation vs. Peak EF (modeling)

	TMS hotspot			Peak EF		
Subject ID	x	y	z	x	y	z
MGS001	-42	-38	68	-54	-28	56
MGS003	-38	-42	74	-54	-9	58
MGS005	-54	-5	55	-61	-7	47
MGS006	-50	-11	71	-53	-18	66
MGS010	-39	-51	66	-52	-30	57
MGS011	-35	-13	71	-54	-20	65
MGS012	NA	NA	NA	-49	-21	62

TABLE II

Peak electric field Intensity (in V/m) for different conductivity values determined using ROAST software

	0.126 S/m		0.276 S/m		1.654 S/m	
	EF_{WM}	EF_{GM}	EF_{WM}	EF_{GM}	EF_{WM}	EF_{GM}
MGS001	0.126	0.149	0.131	0.1448	0.124	0.1496
MGS003	0.247	0.475	0.247	0.5004	0.258	0.4715
MGS005	0.061	0.136	0.061	0.1352	0.062	0.1331
MGS006	0.150	0.133	0.152	0.1386	0.152	0.1386
MGS010	0.089	0.133	0.093	0.1377	0.092	0.1418
MGS011	0.202	0.164	0.213	0.1663	0.226	0.1534
MGS012	0.196	0.140	0.203	0.2382	0.189	0.1415

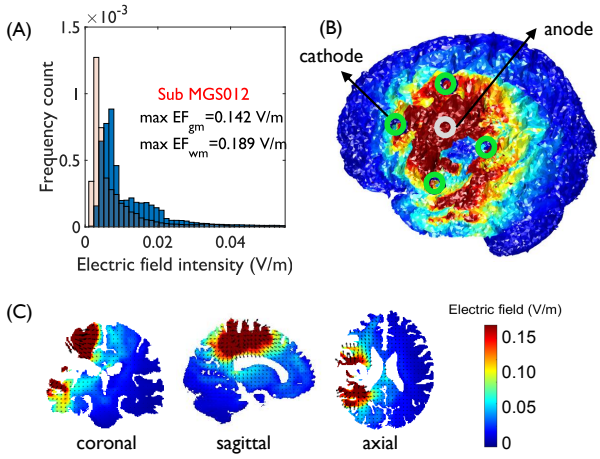

Fig. 3. Simulation results of the current flow modeling in an exemplary subject (MGS012)

In Table I, we present the MNI coordinates of the HMH identified using TMS. One of the subjects (MGS012) did not show any MEP at maximum stimulator output. These coordinates were used for the simulation of current flow in roast. In terms of the localization, the peak EF coordinates (across gray and white matter tissues) had a mean distance (mean ± std: 21.2 mm ± 11.3 mm, range: [9mm, 40.1mm]) from the TMS-derived HMH. This shows that the peak EF coordinates derived from computational modeling can be highly variable across participants. Interestingly, we found that the coordinate of peak EF (based on modeling) was found to be closer to the hand-knob location on the cortex

defined in the literature [17] (MNI coordinate: [-40 -20 50]) (mean distance: 14.3mm ±2.4 mm) as compared to that of TMS-derived HMH (mean distance: 25.4 ± 14.2 mm).

In Table II, the peak electric field intensities (EF_{wm} and EF_{gm} corresponding to the white matter and gray matter within the ipsilesional M1 region) are presented for different conductivity values (0.126 S/m, 0.276 S/m, and 1.654 S/m corresponding to the white matter, gray matter, and CSF respectively). The rationale is that the lesion volume could overlap different tissue masks (WM/GM/CSF). Based on the Wilcoxon ranksum test, we did not find any significant differences in EF values across conductivity values.

We noticed that the within-subject variability in the peak EF magnitude (for different conductivity values of lesion tissue) was less than between-subject variability (for a given conductivity value). We suspect this observation is primarily due to the differences in the hotspot location and anatomical differences due to gray matter and white matter volume across subjects.

IV. CONCLUSIONS AND FUTURE DIRECTION

In this paper, we demonstrated an automated workflow for the computational modeling of current flow upon targeted NIBS in chronic stroke with lesions. The preliminary results suggest that despite using the same configuration in simulating the current flow, the stroke lesion location did not affect the peak EF in the targeted region of interest.

Our study has certain limitations such as: (1) Identifying the lesion mask in an automated manner is not foolproof, as the manual lesion identification by trained radiologists is still considered the gold standard. However, with the current advances in the machine-learning-based segmentation of pathological MRIs, we believe the automated tools will soon surpass the human-level performance, (2) The co-registration of the subject MRI into the MNI template can potentially introduce some registration errors. So, we recommend cautious interpretation of the findings related to the anatomical atlas-based region of interest. (3) To avoid an extensive computational burden, we assume isotropic conductivity values within each tissue in the current computational modeling framework. We recommend the future studies must integrate a computationally tractable framework that considers anisotropic conductivity. With the proposed approach of dose-controlled tDCS in [18] and our workflow to estimate the EF intensity in the presence of lesions, we believe adjusting the dosage for HD-tDCS based precision neurorehabilitation in stroke is possible. As a follow-up to this study, we are currently investigating the localization accuracy in terms of the NIBS motor hotspot and the EEG-based cortical source localization during hand contraction motor tasks in chronic stroke. We hope that the EEG-based source localization and the motor hotspot derived from TMS and tDCS modeling will guide us towards developing personalized motor rehabilitation in stroke. Further, our future work will investigate the effect of the weakened structural integrity of the corticospinal tract on the tDCS current flow as well as functional outcomes of motor tasks. Considering the heterogeneity in stroke characteristics and between-subject EF, future studies designing a personalized NIBS intervention must consider the structural anomalies in the brain.

REFERENCES

[1] O. M. Lapenta, L. M. Marques, G. G. Rego, W. E. Comfort, and P. S. Boggio, "TDCS in Addiction and Impulse Control Disorders," J. ECT, vol. 34, no. 3, pp. 182–192, 2018.

[2] S. Bornheim, A. Thibaut, C. Beaudart, P. Maquet, J. L. Croisier, and J. F. Kaux, "Evaluating the effects of tDCS in stroke patients using functional outcomes: a systematic review," Disability and Rehabilitation. Taylor and Francis Ltd, 2020.

[3] A. Gomez Palacio Schjetnan, J. Faraji, G. A. Metz, M. Tatsuno, and A. Luczak, "Transcranial direct current stimulation in stroke rehabilitation: A review of recent advancements," Stroke Research and Treatment. 2013.

[4] V. S. Handiru, A. P. Vinod, A. K. Keng, E. Chew, and C. Guan, "Effects of transcranial direct current stimulation on the motor-imagery brain-computer interface for stroke recovery: An EEG source-space study," in 2017 IEEE International Conference on Systems, Man, and Cybernetics (SMC), 2017, pp. 2322–2327.

[5] S. Lefebvre and S. L. Liew, "Anatomical parameters of tDCS to modulate the motor system after stroke: A review," Front. Neurol., vol. 8, no. FEB, 2017.

[6] J. P. Dmochowski et al., "Targeted transcranial direct current stimulation for rehabilitation after stroke," Neuroimage, vol. 75, pp. 12–19, 2013.

[7] H. I. Kuo et al., "Comparing cortical plasticity induced by conventional and high-definition 4 × 1 ring tDCS: A neurophysiological study," Brain Stimul., vol. 6, no. 4, pp. 644–648, 2013.

[8] K. Jung et al., "Effective connectivity during working memory and resting states: A DCM study," Neuroimage, vol. 169, no. December 2017, pp. 485–495, 2018.

[9] S. Rossi, M. Hallett, P. M. Rossini, and A. Pascual-Leone, "Screening questionnaire before TMS: An update," Clinical Neurophysiology. 2011.

[10] H. Thair, A. L. Holloway, R. Newport, and A. D. Smith, "Transcranial direct current stimulation (tDCS): A Beginner's guide for design and implementation," Front. Neurosci., vol. 11, no. NOV, pp. 1–13, 2017.

[11] S. Groppa et al., "A practical guide to diagnostic transcranial magnetic stimulation: Report of an IFCN committee," Clinical Neurophysiology, vol. 123, no. 5. Elsevier, pp. 858–882, 01-May-2012.

[12] T. Wagner, F. Fregni, S. Fecteau, A. Grodzinsky, M. Zahn, and A. Pascual-Leone, "Transcranial direct current stimulation: A computer-based human model study," Neuroimage, vol. 35, no. 3, pp. 1113–1124, 2007.

[13] D. Pustina, H. B. Coslett, P. E. Turkeltaub, N. Tustison, M. F. Schwartz, and B. Avants, "Automated segmentation of chronic stroke lesions using LINDA: Lesion identification with neighborhood data analysis," Hum. Brain Mapp., 2016.

[14] M. N. Humberto Mestre, Ting Du, Amanda M. Sweeney, Guojun Liu, Andrew J. Samson, Weiguo Peng, Kristian Nygaard Mortensen, Frederik Filip Stæger, Peter A. R. Bork, Logan Bashford, Edna R. Toro, Jeffrey Tithof, Douglas H. Kelley, John H. Thomas, Poul G. Hjorth, E, "Cerebrospinal fluid influx drives acute ischemic tissue," Science (80)., vol. 367, no. 6483, pp. 1198–1199, 2020.

[15] J. A. Maldjian, P. J. Laurienti, R. A. Kraft, and J. H. Burdette, "An automated method for neuroanatomic and cytoarchitectonic atlas-based interrogation of fMRI data sets," Neuroimage, vol. 19, no. 3, pp. 1233–1239, Jul. 2003.

[16] M. C. Piastra et al., "ASH: an automatic pipeline to generate realistic and individualized chronic stroke volume conduction head models," J. Neural Eng., vol. 18, no. 4, Mar. 2021.

[17] L. Cárdenas-Morales et al., "Network connectivity and individual responses to brain stimulation in the human motor system," Cereb. Cortex, vol. 24, no. 7, pp. 1697–1707, 2014.

[18] C. Evans, C. Bachmann, J. S. A. Lee, E. Gregoriou, N. Ward, and S. Bestmann, "Dose-controlled tDCS reduces electric field intensity variability at a cortical target site," Brain Stimul., vol. 13, no. 1, pp. 125–136, 2020.